In-flight validation of Metis Visible-light Polarimeter Coronagraph on board Solar Orbiter

A. Liberatore[1],[⋆], S. Fineschi[1], M. Casti[2], G. Capobianco[1], L. Abbo[1], V. Andretta[3], V. Da Deppo[4], M. Fabi[5], F. Frassati[1], G. Jerse[6], F. Landini[1], D. Moses[7], G. Naletto[8], G. Nicolini[1], M. Pancrazzi[1], M. Romoli[9], G. Russano[3], C. Sasso[3], D. Spadaro[10], M. Stangalini[11], R. Susino[1], D. Telloni[1], L. Teriaca[12], and M. Uslenghi[13]

[1] INAF - Astrophysical Observatory of Turin, Italy
[2] The Catholic University of America at NASA-GSFC, USA
[3] INAF - Astronomical Observatory of Capodimonte, Naples, Italy
[4] CNR - IFN, Padua, Italy
[5] University of Urbino Carlo Bo and INFN, Florence, Italy
[6] INAF - Astrophysical Observatory of Trieste, Italy
[7] U.S. Naval Research Laboratory, Washington, USA
[8] University of Padua, Italy
[9] University of Florence, Italy
[10] INAF - Astrophysical Observatory of Catania, Italy
[11] ASI - Italian Space Agency, Rome, Italy
[12] MPS, Göttingen, Germany
[13] INAF - IASF, Milan, Italy

ABSTRACT

Context. The Metis coronagraph is one of the remote-sensing instruments of the ESA/NASA Solar Orbiter mission. Metis is aimed at the study of the solar atmosphere and solar wind by simultaneously acquiring images of the solar corona at two different wavelengths; visible-light (VL) within a band ranging from 580 nm to 640 nm, and in the HI Lyα 121.6 ± 10 nm ultraviolet (UV) light. The visible-light channel includes a polarimeter with electro-optically modulating Liquid Crystal Variable Retarders (LCVRs) to measure the linearly polarized brightness of the K-corona to derive the electron density.

Aims. In this paper, we present the first in-flight validation results of the Metis polarimetric channel together with a comparison to the on-ground calibrations. It is the validation of the first use in deep space (with hard radiation environment) of an electro-optical device: a liquid crystal-based polarimeter.

Methods. We used the orientation of the K-corona's linear polarization vector during the spacecraft roll maneuvers for the in-flight calibration.

Results. The first in-flight validation of the Metis coronagraph on-board Solar Orbiter shows a good agreement with the on-ground measurements. It confirms the expected visible-light channel polarimetric performance. A final comparison between the first pB obtained by Metis with the polarized brightness (pB) obtained by the space-based coronagraph LASCO and the ground-based coronagraph KCor shows the consistency of the Metis calibrated results.

Key words. Solar Orbiter – Metis – coronagraph – Sun – Solar corona – Polarimeter – Liquid Crystal Variable Retarder – in-flight calibration

1. Introduction

The Sun is our only opportunity to study in detail magnetically driven activity in solar-like and late main sequence stars. Moreover, the diagnostics of the physical parameters of the coronal magnetized plasma is a crucial tool for understanding phenomena that can affect the Earth magnetosphere. For this reason, many space missions aim to take data about our star.

Solar Orbiter is one of those missions.[1] The scientific goal is to perform detailed measurements of the inner heliosphere and solar wind by combining observations from all the 10 on-board instruments. Solar Orbiter will allow for the first time the remote-sensing observation of the Sun from as close as 0.28 AU. Thanks to several gravitational assists with Venus and Earth, the spacecraft inclination will be increased with respect to the ecliptic plane until ≈ 30° allowing Solar Orbiter to observe the Sun's polar regions (Müller et al. 2020). Among the Solar Orbiter remote-sensing instruments, there is the Metis[2] coronagraph for the study of the solar corona (Antonucci et al. 2020; Fineschi et al. 2020).

One of the observational goals of Metis is the measurement of the linear polarization of the Kontinuum component of the corona (K-corona). The K-corona is due to the Thomson diffusion by the coronal free electrons of the photospheric radiation

[2] In the ancient Greek mythology, Metis was the symbol of wisdom and deep thought.

and it is linearly polarized (e.g., Inhester 2016, Raouafi 2011). The coronal emission is optically thin and contains not only the linearly polarized K-corona but also a mostly unpolarized component due to the scattering of photospheric light from dust (F-corona). Instrumental stray light would also adds up to the coronal signal. In order to eliminate these components, Metis will measure the polarized brightness (pB) through the acquisition of four images with different polarization angle. A polarimeter assembly is situated along the optical path of the visible channel with the presence of an electro-optically modulating Liquid Crystal Variable Retarder (LCVR). From the images of the K-corona polarized brightness a map of the coronal electron density can be derived. (Van De Hulst 1950) This coronal plasma quantity is essential to obtain other parameters, such as the solar wind speed, to help determining the origin and acceleration of the solar wind.

In Section 2, we describe more in detail the Metis coronagraph and its polarimeter assembly comprising the LCVR. Section 3 presents the first in-flight validation results of the Metis LCVR. In Section 4, we report the pB cross-calibration between Metis and SOHO/LASCO.

2. Metis coronagraph

Metis is the coronagraph on-board Solar Orbiter for the observation of the inner corona, that is, within heliocentric heights < 9 solar radii ($R_\odot$). During the mission, the spacecraft will cover a wide range of distances from the Sun. For this reason, all the instruments aboard have a particular design to deal with a high thermal flux when they are at the perihelion. In order to reduce the high thermal load on the instrument when it is near the Sun, the Metis occultation scheme was based on an "inverted" externally-occulted configuration. The coronal light is collected by an on-axis aplanatic Gregorian telescope while the Sun-disk light is rejected by a mirror put along the path (M0 in Fig. 1). The inverted external-occulter (IEO) consists of a circular aperture that reduces by two orders of magnitude the thermal load on the rejection mirror compared to that in the annular aperture of classical coronagraphs (Fineschi et al. 2020).

Metis can simultaneously acquire images in visible and ultraviolet light (Fig. 1). The coronal light is splitted by a UV interferential filter that works by selecting the UV Ly$_\alpha$ (121.6 nm) in transmission and by reflecting the visible-light (VL) to the polarimeter passing through a bandpass filter at $580 - 640$ nm. All the details about the optical design and performance can be found in Refs. (Antonucci et al. 2020) (Fineschi et al. 2020).

The VL optical path comprises a polarimeter assembly with two electro-optically modulating Liquid Crystals Variable Retarders[3] (Fig. 2). (Fineschi et al. 2005) (Zangrilli et al. 2009) An LCVR consists of optically anisotropic liquid crystal molecules embedded between two glasses with a conductive film with an ordered orientation. They have an effective birefringence value that can be changed by applying an electric field to the cells that rotates the molecules. LCVRs technology has many advantages and this is the first time that is used in a space mission.[4] Retarders based on liquid crystals do not use moving mechanical parts, reducing noise, failure probability, and mass. The power
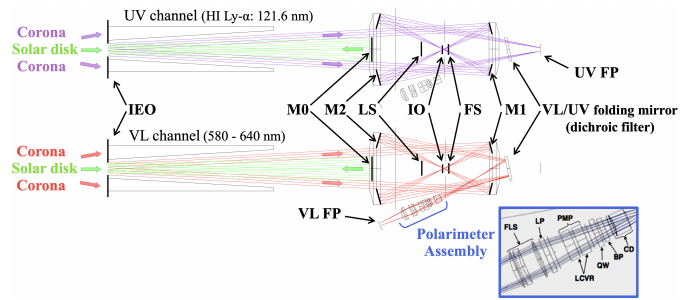

Fig. 1. Metis ray trace for the UV and VL channels. The Sun-disk light is rejected by the mirror M0 while the coronal light is collected by an on-axis aplanatic Gregorian telescope. The suppression of the diffracted light off the edges of the IEO and M0 is achieved, respectively, with an internal occulter (IO) and a Lyot trap (LS). The polarimeter consists of the following elements: a collimating doublet (CD), a VL bandpass filter (BP), a focus lens system (FLS), a quarter-wave (QW) plate retarder, a polarization modulation package (PMP) comprising two liquid crystals variable retarders (LCVRs), a linear polarizer (LP) and a focusing lens system (FLS). On the focal planes (FP) are positioned the detectors.

consumption of the liquid crystal-based retarders is reduced and their response is very fast (of the order of milliseconds), providing in this way a fast modulation of the polarization state of light.
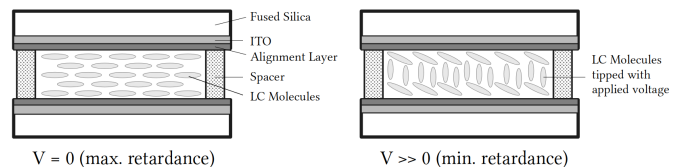

Fig. 2. Schematic representation of a Liquid Crystal Variable Retarders operation.

LCVR devices are sensitive to temperature (Fig. 3). Indeed, the retardance depends on the temperature of the liquid crystals cells because the different temperatures can facilitate (if higher) or contrast (if lower) the rotation of the molecules. For this reason, Metis Polarization Modulation Package (PMP) has a temperature controller to guarantee the temperature stability on liquid crystal cells. Nominally, the LCVR works at a temperature of 30°C. However, a characterization of the LCVR performance at different temperatures was also performed during the on-ground calibrations and can be found in (Casti et al. 2018).

The on-ground calibration yielded the Metis polarimeter demodulation tensor $\mathbf{X}^\dagger$. This tensor is obtained by computing and inverting the modulation matrix $\mathbf{X}$ associated with each pixel of the acquired polarimetric images. The elements of these demodulation matrices are collected in images, each relating to an element of the matrix (obtaining a tensor of 12 images, considering that the demodulation matrices have dimension 3×4, see Eq. 3).

The demodulation tensor polarimetrically characterises the incoming light by returning its Stokes vector $\mathbf{S} = (S_0, S_1, S_2) = (I, Q, U)$.[5] In accordance with the considered Polarimeter Instru-

---

[3] The LCVR cells that compose the Metis PMP have been assembled with the fast axes aligned and the pre-tilt angle of the liquid crystal molecules in opposite direction, in order to obtain a wider acceptance angle (equal to $\pm 4°$). (Alvarez-Herrero et al. 2011) (Casti et al. 2018)

[4] It is used also in the Polarimetric and Helioseismic Imager (PHI) instrument on-board Solar Orbiter (Solanki et al. 2020).

[5] The K-corona is linearly polarized due to the Thomson scattering of the solar disk radiation by the free electrons in the coronal medium. Being the fourth Stokes parameter ($S_3 \equiv V$) associated with circular polarization, we can consider just the first three Stokes parameters $(S_0, S_1, S_2) \equiv (I, Q, U)$ and set $V = 0$.
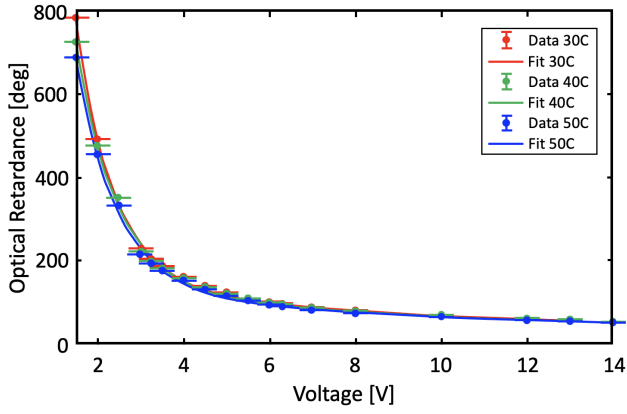
Fig. 3. Optical retardances for different applied voltages and verification of the PMP performance for different temperatures. (Casti et al. 2018)
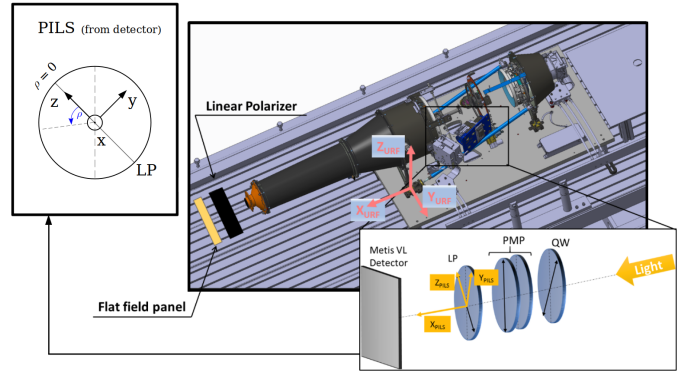

Fig. 4. Schematic view of the set up used for data acquisition and Metis polarimeter optical elements relative orientations in PILS reference frame [compared with the Unit Reference Frame (URF)]. The arrows in the optical elements represent, respectively: the fast axes for both the QW and the LP, and the PMP polarization axis.

ment Level System (PILS) reference france PILS[6] (Fig. 5) we can define the these Stokes parameters as:

$I \equiv$ Intensity of the linearly polarized radiation beam along $\hat{n}_{Z_{PILS}}$ plus
    intensity of linearly polarized radiation along $\hat{n}_{Y_{PILS}}$:
$$I_{\hat{n}_{Z_{PILS}}} + I_{\hat{n}_{Y_{PILS}}}$$

$Q \equiv$ Intensity of linearly polarized radiation along $\hat{n}_{Z_{PILS}}$ minus intensity
    of linearly polarized radiation along $\hat{n}_{Y_{PILS}}$:
$$I_{\hat{n}_{Z_{PILS}}} - I_{\hat{n}_{Y_{PILS}}}$$

$U \equiv$ Intensity of linearly polarized radiation along $(\hat{n}_{Z_{PILS}} + \hat{n}_{-Y_{PILS}})/\sqrt{2}$
    minus intensity of linearly polarized radiation along $(\hat{n}_{Y_{PILS}} + \hat{n}_{Z_{PILS}})/\sqrt{2}$:
$$I_{(\hat{n}_{Z_{PILS}} + \hat{n}_{-Y_{PILS}})/\sqrt{2}} - I_{(\hat{n}_{Y_{PILS}} + \hat{n}_{Z_{PILS}})/\sqrt{2}}$$

where $\hat{n}_{X_{PILS}}$, $\hat{n}_{Y_{PILS}}$, and $\hat{n}_{Z_{PILS}}$ are the unit vectors parallel to the x, y, and z-axis in the PILS reference frame. From the Stokes parameters it is possible to define the polarized brightness:

$$pB = \sqrt{Q^2 + U^2} \qquad (1)$$

Four images $\mathbf{m} = [m_1, m_2, m_3, m_4]$ at different retardance values are obtained by varying the voltage applied to the LCVRs and then they are combined through the relation $\mathbf{m} = \mathbf{XS} \rightarrow \mathbf{S} = \mathbf{X}^\dagger \mathbf{m}$. Where the theoretical modulation matrix is given by Eq. 2 as follow:

$$\mathbf{X} = \frac{1}{2}\begin{pmatrix} 1 & \cos\delta_1 & \sin\delta_1 \\ 1 & \cos\delta_2 & \sin\delta_2 \\ 1 & \cos\delta_3 & \sin\delta_3 \\ 1 & \cos\delta_4 & \sin\delta_4 \end{pmatrix} = \frac{1}{2}\begin{pmatrix} 1 & 0 & 1 \\ 1 & -1 & 0 \\ 1 & 0 & -1 \\ 1 & 1 & 0 \end{pmatrix} \qquad (2)$$

where the values of the quadruplet retardances, δ_i, $i = 1, 2, 3, 4$, of the LCVR in the polarimeter are $\delta_1 = 90°$, $\delta_2 =$

---

[6] X$_{PILS}$ = parallel to the incoming light direction, pointing the VL detector; Z$_{PILS}$ = parallel to the Metis linear polarise acceptance axis; Y$_{PILS}$ = to complete the right handed reference system.

180°, $\delta_3 = 270°$, $\delta_4 = 0°$. The theoretical demodulation matrix $\mathbf{X}^\dagger$ (Eq. 3) is obtained as the Moore-Penrose inverse of the theoretical modulation matrix $\mathbf{X}$.

$$\mathbf{X}^\dagger = \frac{1}{2}\begin{pmatrix} 1 & 1 & 1 & 1 \\ 0 & -2 & 0 & 2 \\ 2 & 0 & -2 & 0 \end{pmatrix} \qquad (3)$$

As mentioned, the experimental demodulation tensor associated with the Metis polarimeter was derived during the on-ground calibration by acquiring images of a known polarized source modulated by applying different voltages to the LCVR cell. By considering the elements of the Stokes vectors associated to the known polarized source (generated by a rotating linear pre-polarizer), a linear system was solved for each detector pixel to derive the demodulation tensor (Casti et al. 2018; Liberatore et al. 2021). More information about the on-ground calibration of the Metis VL polarimetric channel can be found in Refs. (Casti et al. 2019), (Fineschi et al. 2020).

3. Polarimeter in-flight validation

In this section we analyze the in-flight validation of the Metis polarimeter carried out during the first image acquisitions by the Metis coronagraph.

3.1. LCVR retardances evaluation

The K-corona is due to the Thomson diffusion of the photospheric radiation by the coronal free electrons in the solar atmosphere. It is linearly polarized and the polarization vector is tangent to the solar limb. These properties of the K-corona polarization vector can be used to perform the in-flight validation of the LCVR retardances.

The K-corona polarization vector crossing the transmission axis of the polarimeter analyzer with an angle, the "polar angle", α, shown in Fig. 5, results in an intensity modulation in each single $i - th$ image of the set of 4 coronal images, acquired at different voltages of the polarimeter. This modulation is calculated from the recorded signal, m_i, for each sensor element $P(r, \alpha)$ de-

trended of the total intensity, $I^{(0)}$, and normalized by the $pB^{(0)}$ (Elmore et al. 2000):

$$\frac{2m_i - I^{(0)}}{pB^{(0)}} = \cos[2(\alpha - \rho_i)] \tag{4}$$

where m_i are the in-flight data and the angles ρ_i are equivalent to effective polariser rotations equal to half the LCVR's retardances, $\rho = \delta/2$. The initial evaluations of $I^{(0)}$ and $pB^{(0)}$ are carried out by using the ground calibrated effective polariser rotation angles, $\rho_i^{(0)} = \delta_i^{(0)}/2$. The in-flight retardance values, δ_i, are retrieved through the following 3-parameters (P0, P1, P2) regression:

$$y_i = P_0 + P_1 \cos\left[2(x - P_2)\right] \tag{5}$$

where $y_i = (2m_i - I)/pB$, x is the polar angle α, P_0 is the bias of fitting curve, and P_1 is the modulation amplitude. The P_2 parameter is defined as:

$$P_2 = \rho_i - 45° \tag{6}$$

where the shift of $-45°$ is introduced to align the PILS reference frame with the solar coordinate system (aligning the z_{PILS}-axis with the solar East-West direction; Fig. 5).
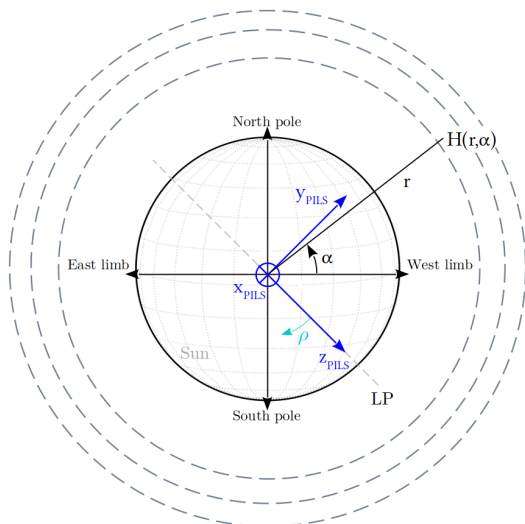

Fig. 5. Positions on the sensors elements, $H(r, \alpha)$, for the LCVR retardances evaluation in Eq. 5. We considered different heliocentric distances, r, from 3.14 $R_\odot$ to 3.63 $R_\odot$ and different polar angles, α. The PILS reference frame position relative to the Sun is shown in blue (in particular, the z_{PILS} axis results to be at -45° from the West solar limb).

A regression is calculated for each y_i obtained from the respective image of the quadruplet m_i, for a fixed distance from the center of the Sun as obtained by astrometry (Fig. 6).

The P_2 parameters give the polarization angles ϑ for different heliocentric heights. We considered 10 heliocentric distances from 3.14 $R_\odot$ to 3.63 $R_\odot$ from the Sun center (SC) in order to avoid noisy regions at the inner and outer edges of the field-of-view (Fig. 5). The expected average values from ground calibration for the nominal quadruplet polarization, ρ_i, are: (49.1°, 84.3°, 133.2°, 181.1°) with an pixel-by-pixel, flat-field uncertainty ±5° each (Q4 in Table 2). From the average of the values at different heliocentric heights, we obtain: ($\rho_1 = 45.0° \pm 0.1°$,
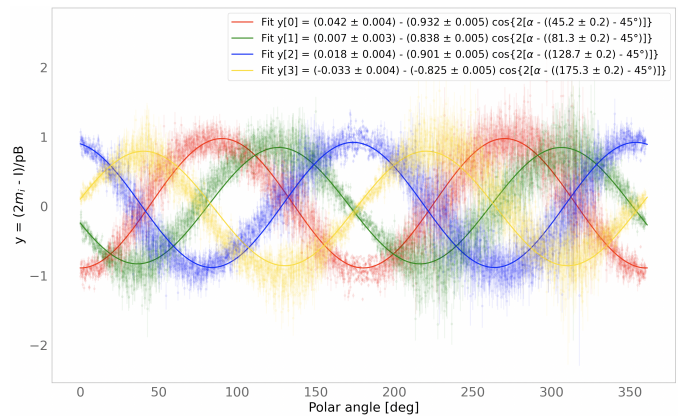

Fig. 6. Intensity modulation in each $i-th$ image of the polarization set of 4 coronal images, expressed in Eq. 4, as a function of the "polar angle", α, shown in Fig. 5. The LCVR retardances, δ_i, were derived from the regression in Eq. 5. The data come from a quadruplet acquired during the "roll n.0" of the IT-7 campaign (on June 8th, 2020 - Fig. 8) for a fixed heliocentric height (620 pixels from the Sun center in this particular case).

$\rho_2 = 81.4° \pm 0.1°$, $\rho_3 = 128.7° \pm 0.1°$, $\rho_4 = 175.4° \pm 0.1°$). The errors are obtained from the sinusoidal fits (6).

The values of the retardances of the LCVR measured in-flight are within the uncertainty, due to the flat field, in the retardances derived on-ground.

Even if these values have a lower error than those obtained during the on ground calibration, it was decided to continue to use the latter ones because they were obtained through a pixel by pixel process (through the use of a demodulation tensor). On the other hand, the in-flight ones were evaluated only for some fixed heliocentric heights and polar angles. However, the obtained result shows the consistency between the on-ground and the in-flight results. It is the first in-flight validation of a polarimeter with liquid crystal-based polarimeter. It may be useful to repeat this process in the future to check the status of the polarimeter over time.

3.2. Different voltage configurations

During the first remote sensing checkout window (RSCW1 - June 18th, 2020 - distance to the Sun: 0.52 A.U.), we acquired polarimetric sequences with different quadruplets of PMP voltages. A quadruplet consists of 4 images at 4 LVCR voltages (i.e., effective "polarization angles") separated by $\approx 45°$ from each other. The ground calibration yielded the demodulation tensor associated to each of these quadruplets (in addition to the nominal one). The goal of these different acquisitions is to check the polarimeter's response for the other set of 4 voltage configurations. Table 2 summarises the considered quadruplets, with an effective angle error of $\approx 1°$.

The demodulation tensor associated with each considered quadruplet returns the corresponding $pB^{(1)}$, that are refined values with respect to the initial $pB^{(0)}$ obtained from the ground-calibrated quadruplets[7]. In the following, these refined values of polarized brightness will be indicated as $pB \equiv pB^{(1)}$, for short. Considering 4 different coronal regions (near the streamers -Region 1, 3- and near coronal holes -Region 2, 4-) and perform-

---

[7] In particular we have 5 pB because we performed two acquisitions with "quadruplet 4".

ing an average over the pixels inside these regions (Fig. 7), we can compare the measured pB with different voltage configurations. The resulting pB should be the same for each configuration. Fig. 7 shows that the differences between the pB returned by different quadruplets are $\leq 2\%$.
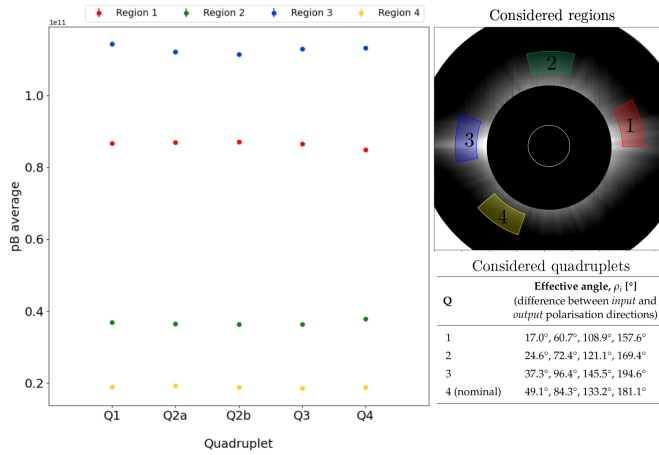

Fig. 7. Comparison between the average of the four pB regions for the different quadruplets Q_i (see Table 2). The differences between the different pB are less than 2%.

4. Validation during spacecraft roll

We acquired different image sets during a complete roll performed by the spacecraft on June 8th, 2020 (IT-7 campaign; S/C - Sun distance: 0.52 A.U.). During the roll maneuver, the Metis polarimeter acquired a total of 8 K-corona pB images (one for each roll position - see Fig. 8). The comparison among these images gives the differences in the polarimetric response at different positions across the polarimeter and the detector.

The Degree of Linear Polarization (DoLP) is derived from the ratio between pB and the first Stokes parameter I. Fig. 8 shows the pB/I images for different spacecraft roll positions. For a few selected coronal regions on the frame (for example along a streamer), at different heliocentric distances (the Sun's center position behind the internal occulter is derived from astrometry measurements), the pB/I is plotted as a function of roll angle.
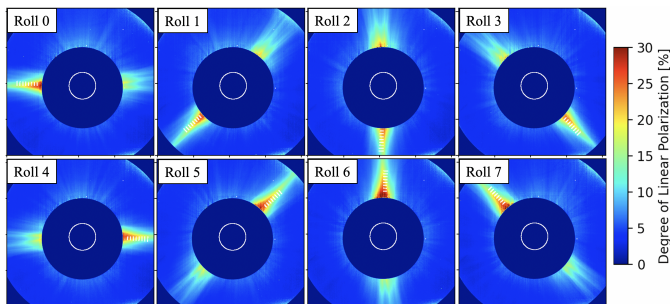

Fig. 8. Degree of linear polarization (pB/I) of the K-corona for the eight different S/C roll positions and considered region (white rectangles) to evaluate the polarimetric flat field goodness. The white circle inside the internal occulter show the Sun size and position.

4.1. Check on the LCVR retardances during S/C roll

By analizing the data acquired during the spacecraft rolls, we can repeat the same type of analysis performed in Subsec. 3.1. For a given region in the solar corona, the spacecraft roll acts as a "rotating polarizer". Thefore, the recorded intensity of a selected region follows the Malus's law (Fig. 9). The fitting parameters of this function give an estimation of the LCVR retardances that can be compared with those measured from the ground calibration and with those obtained from the previous method.

Table 1 summarizes the retardances measured with the on-ground calibration, with the Malus curve fitting Eq. 4 (cfr., Fig. 6), and with the Malus curve obtained from the roll maneuver (cfr., Fig. 9).
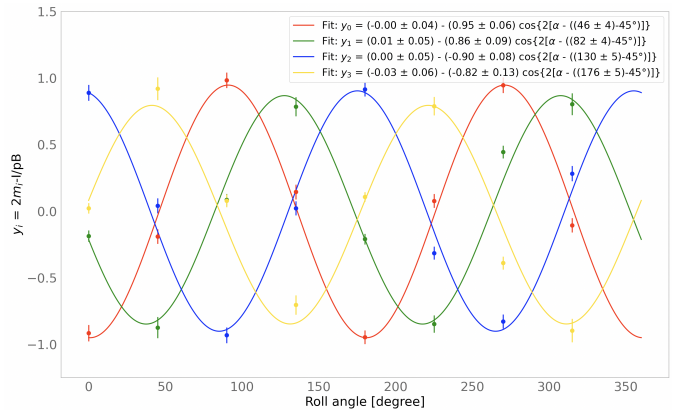

Fig. 9. Malus curve obtained from $y_i = (2m_i - I)/pB$ average values over the pixels in a fixed region in the solar corona during each roll.

Table 1. Comparison between the LCVR polarization angles from on-ground calibration and in-flight validation.

Theo.	On-ground	In-flight (polar angle, Fig. 6)	In-flight (roll maneuver, Fig. 9)
45	49°± 5°	45.0° ± 0.1°	46° ± 4°
90	84°± 5°	81.4° ± 0.1°	82° ± 4°
135	133°± 5°	128.7° ± 0.1°	130° ± 5°
180	181°± 5°	175.4° ± 0.1°	176° ± 5°

4.2. Polarized flat field verification

We verified in flight the polarized flat field by considering the pB of coronal structures measured as they moved to different locations across the detector, during roll maneuvers of the Solar Orbiter spacecraft as shown in Fig. 8.

Fig. 10 shows, as a function of roll angle, the pB/I derived from the demodulation tensor, $X^{\dagger}$, measured during the on-ground calibrations. The quality of the polarization flat-fielding obtained by applying the on-ground calibrated demodulation tensor is indicated by the constant pB/I values (i.e., < 5%; except for the heliocentric height 3.39 R$_\odot$, with percentage variation ∼ 12%), for different roll angles, the same heliocentric height.

The degree of linear polarization decreases for increasing heliocentric distances: from (0.24 ± 0.01) at $3.39\,R_\odot$ to (0.14 ± 0.01) at $4.91\,R_\odot$. Is it possible to notice that, at higher heliocentric heights, the behavior of pB/I during the roll maneuvers results to be less flat due to the decrease of the S/N.

As a comparison, Fig. 11 shows, as a function of roll angle, the pB/I derived from the theoretical demodulation tensor $X^\dagger$ given by Eq. 3. The uncertainty of the pB/I mean values using the theoretical $X^\dagger$ is from a factor of two to three higher than those using the demodulation tensor from the on-ground calibration. Table 3 summarises the pB/I values for the two cases.

Data reduction with the theoretical $X^\dagger$ would return the signal state of polarization, pB/I, with an accuracy of only about 10% (best case). This would be the dominant uncertainty considering that the one due to the uncertainty of the pB/I is $\approx 2\%$, in the considered regions. On the other hand, with the experimental $X^\dagger$ the uncertainty in deriving the pB/I values drops to $< 5\%$. This is comparable to the $\approx 3\%$ error of $\approx 1\% - 3\%$ due to the data uncertainty. In conclusion, the experimental demodulation tensor from ground calibration returns polarization measurements with an accuracy of $< 5\%$. As estimated in (Fineschi et al. 2005), with an accuracy of $\approx 1\%$ on the pB (to be compared with the obtained 1-3% due to data uncertainty), we can expect an 1% error on the electron density evaluation.
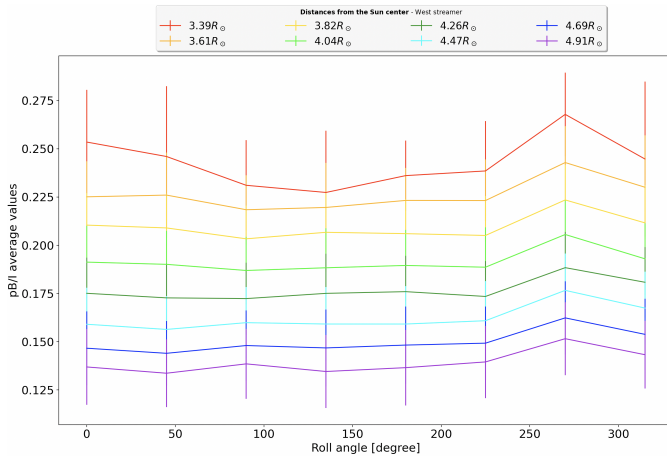

Fig. 10. pB/I average over the pixels inside the selected regions (for each roll) by using the demodulation tensor obtained during the ground calibration. The bars represent the intensity uncertainty inside the considered area.

The retardances calculated from the fitting of the Malus's curves acquired during the spacecraft rolls are: ($46°\pm4°$, $82°\pm4°$, $130° \pm 5°$, $176° \pm 5°$).

5. Metis first light pB comparison

A preliminary verification of the in-flight validation was obtained from the comparison of the coronal polarized brightness as measured by Metis with that obtained by other instruments. In particular, we compared the Metis pB with that of the K-Cor (Hou et al. 2013) and LASCO C2/C3 coronagraphs (Brueckner et al. 1995). We performed this comparison by using the data of May 15th, 2020. At this time Solar Orbiter was almost along the Sun-Earth axis and for this reason LASCO C2 and C3, K-Cor and Metis could be considered aligned (Fig. 12). LASCO-C3 data were available only on the 14th and 16th of May, 2020. Fig. 13, shows the Metis pB value compared to the LASCO and
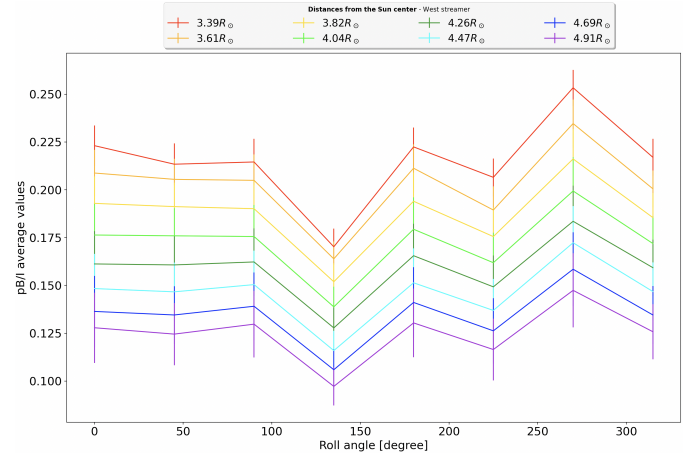

Fig. 11. pB/I average over the pixels inside the selected regions by using the theoretical demodulation tensor. The bars represent the uncertainty inside the considered area.

KCor measurements. On the East streamer Metis pB values are in agreement with those of LASCO-C3, while it is less than a factor of two higher than that of LASCO-C2. On the other hand, on the West limb, Metis and LASCO-C2 measured values agree better. As the Solar Orbiter mission will progress, more Metis pB measurements will allow a refinement of the cross-calibration with other instruments. These initial measurements were a first check of the performances of the Metis polarimeter, and they succeeded in confirming the validity of its on-ground and in-flight validation. (Fineschi et al. 2021).
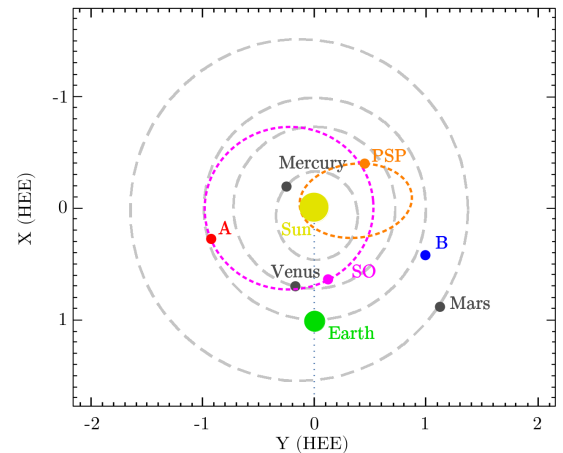

Fig. 12. Position of SolO (SO), STEREO-A (A) and Parker Solar Probe (PSP) with respect to Earth, on May 15, 2020 (00:00 UT). From STEREO webpage.

6. Conclusion

After a summary of the Metis on-ground calibration, we report its first in-flight validation.

The first step was the validation of the LCVR retardances. We considered the geometry of the physical process that polarizes the K-Corona radiation with a polarization vector tangent to the solar limb. At four LCVR retardances values, we acquired four images from which we obtain four Malus curves. From
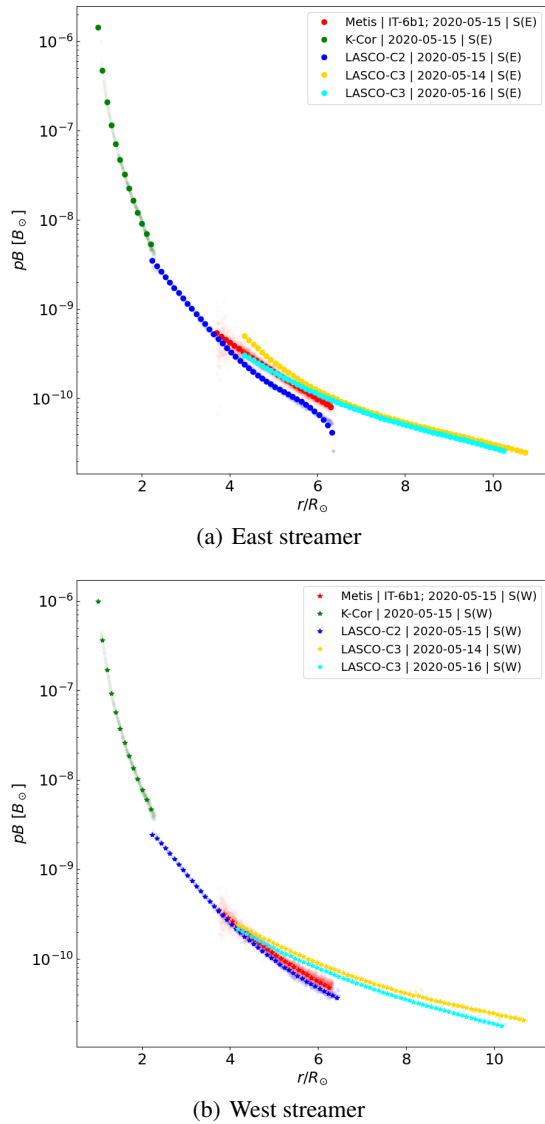
(a) East streamer

(b) West streamer

Fig. 13. Comparison of *pB* values along the East and West streamer between Metis, LASCO C2/C3 and K-Cor instruments during an almost Sun-S/C-Earth alignment (data: 2020-05-15; Sun-S/C distance: 0.64 A.U.).(Fineschi et al. 2021)

these curves we were able to derives the effective LCVR retardances. We obtain retardances, that is, "polarization angles" of: $(45.0° \pm 0.1°, 81.4° \pm 0.1°, 128.7° \pm 0.1°, 175.4° \pm 0.1°)$. We also considered a fixed region in the solar corona during a complete S/C rotation as ulterior check. This gives the same result as "rotating the polarizer". We obtain: $(46° \pm 4°, 82° \pm 4°, 130° \pm 5°, 176° \pm 5°)$ that are consistent with the on ground calibration and with what we obtained by considering the polarization of the K-Corona tangent to the solar limb.

We acquired polarimetric sequences with different quadruplets of the used LCVR voltages to evaluate the polarimetric response at different voltage configurations. We considered four fixed coronal regions and obtained the polarized brightness by using the demodulation tensor associated with each quadruplet. This *pB* comparison from quadruplets with different applied tensions to the polarimeter yielded differences within $\leq 2\%$.

We also evaluated the polarimetric flat field by considering a given coronal regions as it was imaged across different locations of the detector focal plane, during a complete S/C roll. In par-

ticular, we considered different heliocentric heights in the *pB/I* images. As expected, these values have a small percentage variation (i.e., < 5%) at the same heliocentric height during the roll manoeuvre. The percentage variation of the *pB/I* mean values using the theoretical demodulation tensor is higher than the one obtained using the on ground calibrations. Quantitatively, by using the demodulation tensor from ground calibration, the accuracy in the polarization measurement improves by a factor of ≈ 3. Indeed, the accuracy of the *pB/I* values by using the theoretical $X^\dagger$ is about 10% while, by using the $X^\dagger$ obtained during on ground calibration, we have an accuracy of $3-5\%$ in the *pB/I* values.

Finally, a comparison of Metis polarized brightness with what obtained by other instruments (LASCO C2 and C3 K-Cor) confirms the goodness of the Metis polarimeter calibration.

References

Alvarez-Herrero, A., Uribe-Patarroyo, N., Parejo, P. G., et al. 2011, in Polarization Science and Remote Sensing V, ed. J. A. Shaw & J. S. Tyo, Vol. 8160, International Society for Optics and Photonics (SPIE), 312 – 329
Antonucci, E., Romoli, M., Andretta, V., et al. 2020, Astronomy & Astrophysics, 642, A10
Brueckner, G. E., Howard, R. A., Koomen, M. J., et al. 1995, Sol. Phys., 162, 357
Casti, M., Fineschi, S., & et al. 2018, in Calibration of the liquid crystal visible-light polarimeter for the Metis/Solar Orbiter coronagraph, ed. M. Lystrup, H. A. MacEwen, G. G. Fazio, N. Batalha, N. Siegler, & E. C. Tong, Vol. 10698, International Society for Optics and Photonics (SPIE), 930 – 943
Casti, M., Fineschi, S., & et al. 2019, in International Conference on Space Optics — ICSO 2018, ed. Z. Sodnik, N. Karafolas, & B. Cugny, Vol. 11180, International Society for Optics and Photonics (SPIE), 1255 – 1269
Elmore, D. F., Card, G. L., Lecinski, A. R., et al. 2000, in Society of Photo-Optical Instrumentation Engineers (SPIE) Conference Series, Vol. 4139, Calibration procedure for the polarimetric instrument for Solar Eclipse-98, ed. S. Fineschi, C. M. Korendyke, O. H. Siegmund, & B. E. Woodgate, 370–377
Fineschi, S., Naletto, G., Romoli, M., & et al. 2020, Experimental Astronomy, 49
Fineschi, S., Romoli, M., Andretta, V., et al. 2021, in Society of Photo-Optical Instrumentation Engineers (SPIE) Conference Series, Vol. 11852, Society of Photo-Optical Instrumentation Engineers (SPIE) Conference Series, 1185211
Fineschi, S., Zangrilli, L., Rossi, G., et al. 2005, in Society of Photo-Optical Instrumentation Engineers (SPIE) Conference Series, Vol. 5901, Solar Physics and Space Weather Instrumentation, ed. S. Fineschi & R. A. Viereck, 389–399
Hou, J., de Wijn, A. G., & Tomczyk, S. 2013, ApJ, 774, 85
Inhester, B. 2016, arXiv: Solar and Stellar Astrophysics, v2, 104
Liberatore, A., Fineschi, S., Casti, M., et al. 2021, in International Conference on Space Optics — ICSO 2020, ed. B. Cugny, Z. Sodnik, & N. Karafolas, Vol. 11852, International Society for Optics and Photonics (SPIE), 1793 – 1814
Müller, D., St. Cyr, O. C., Zouganelis, I., et al. 2020, Astronomy & Astrophysics, 642, A1
Raouafi, N. E. 2011, in Astronomical Society of the Pacific Conference Series, Vol. 437, Solar Polarization 6, ed. J. R. Kuhn, D. M. Harrington, H. Lin, S. V. Berdyugina, J. Trujillo-Bueno, S. L. Keil, & T. Rimmele, 99
Solanki, S. K., del Toro Iniesta, J. C., Woch, J., et al. 2020, A&A, 642, A11
Van De Hulst, H. C. 1950, B.A.N., 11, 135
Zangrilli, L., Fineschi, S., & Capobianco, G. 2009, in Society of Photo-Optical Instrumentation Engineers (SPIE) Conference Series, Vol. 7438, Solar Physics and Space Weather Instrumentation III, ed. S. Fineschi & J. A. Fennelly, 74380W

Table 2. Retardances of the different LCVR quadruplets "Q" (Liberatore et al. 2021).

Q	Effective angle, ρ_i [°] (difference between *input* and *output* polarization directions)	Applied voltage [mV]
1	17.0°, 60.7°, 108.9°, 157.6°	30583, 13216, 8344, 6597
2	24.6°, 72.4°, 121.1°, 169.4°	25362, 11359, 7776, 6313
3	37.3°, 96.4°, 145.5°, 194.6°	19573, 9087, 6924, 5810
4 (nominal)	49.1°, 84.3°, 133.2°, 181.1°	15837, 10048, 7318, 6051

Table 3. pB/I average values with standard deviation (pB and I obtained through the on-ground demodulation tensor [left] and theoretical one [right]). Uncertainty column contains the standard deviation obtained considering the pB/I values in the region at fixed heliocentric distance (white squares in Fig. 8) for each roll.

Roll	On ground $X^\dagger$ (4.26 R$_\odot$) Best case		On ground $X^\dagger$ (3.39 R$_\odot$) Worst case		Theoretical $X^\dagger$ (4.26 R$_\odot$) Best case	
	pB/I	σ	pB/I	σ	pB/I	σ
0	0.175	0.018	0.253	0.027	0.161	0.017
1	0.173	0.018	0.246	0.036	0.160	0.015
2	0.172	0.019	0.231	0.023	0.162	0.017
3	0.175	0.021	0.227	0.031	0.128	0.010
4	0.176	0.019	0.236	0.018	0.166	0.017
5	0.173	0.018	0.239	0.026	0.149	0.016
6	0.188	0.019	0.268	0.022	0.184	0.019
7	0.180	0.018	0.245	0.040	0.159	0.014
Avg.	0.177	0.019	0.243	0.028	0.159	0.016
StD.	0.005	0.001	0.013	0.008	0.016	0.002
StD/Avg	3%	1%	5%	3%	10%	2%